# Black Sea Journal of Engineering and Science

# EFFECTS OF GEOMETRIC PARAMETERS OF PERFORATED DIFFUSER ON SOUND PRESSURE LEVEL SOURCED BY AIRFLOW

**Ahmet ERDOĞAN[1]\*, İshak Gökhan AKSOY[1], Suat CANBAZOĞLU[2]**

[1]*İnönü University, Faculty of Engineering, Department of Mechanical Engineering, 44280, Malatya, Türkiye*
[2]*Retired scientist, Türkiye*

**Abstract:** This study investigates the aeroacoustic behaviors of a square truncated perforated diffuser under airflow, commonly used in Air Handling Units (AHUs). The design parameters are fundamentally taken into account to unveil the aeroacoustic performance of the diffuser. Initially, unsteady-state Computational Fluid Dynamics (CFD) simulations are conducted based on models that accurately represent the fluid domain of the chamber with the perforated diffuser in the ANSYS Fluent environment. Subsequently, the Ffowcs Williams and Hawkings (FW-H) method integrated into the software is employed to acquire time-dependent signals from microphones placed in three different locations within a perforated diffuser chamber. Finally, the results are converted to a frequency range of 0-1000 Hz using the Fast Fourier Transform (FFT) method, and the SPL values are obtained. The results show that the microphone location is crucially important to determine SPL and the porosity reduction from 0.55 to 0.35 can reduce SPL by approximately 30-40 dB. Variations in wall thickness of the diffuser fluctuated between 5-10 dB at each frequency value.

**Keywords:** Air handling units, Computational fluids dynamic, Perforated diffuser, Sound pressure level, Ansys fluent

**\*Corresponding author:** İnönü University, Faculty of Engineering, Department of Mechanical Engineering, 44280, Malatya, Türkiye
**E mail:** ahmet.erdogan@inonu.edu.tr (A. ERDOĞAN)

| | | |
|---|---|---|
| Ahmet ERDOĞAN | (iD) | https://orcid.org/0000-0001-8349-0006 |
| İshak Gökhan AKSOY | (iD) | https://orcid.org/0000-0002-8798-5847 |
| Suat CANBAZOĞLU | (iD) | https://orcid.org/0000-0002-0166-4824 |

## 1. Introduction

Air Handling Units (AHUs) are crucially important components of Heating, Ventilating, and Air Conditioning (HVAC) systems (Yu et al., 2014). An AHU typically conditions the air by adjusting temperature, humidity, and filtration. The cross-sectional area of fans employed in AHUs is less than the cross-sectional area of chambers situated adjacent to the HVAC equipment's fan, including heating/cooling coils, silencer (sound attenuator), filter, or heat recovery elements (Kamer et al., 2018). The air supplied by the fan is therefore partially in contact with the surfaces of other units. The operating efficiency of AHUs is significantly diminished by this situation. In order to address this issue, a chamber with a perforated diffuser is employed after the fan chamber (Erdoğan, 2017). When utilizing a chamber with a perforated diffuser, it becomes feasible to enhance operational efficiency by minimizing the overall pressure loss in the AHU (Bulut et al., 2011). This is achieved by ensuring a uniform passage of air across all the surfaces of the aforementioned units. Minimizing the total pressure loss in the AHU and achieving homogeneous airflow diffusion to the subsequent unit are crucial aspects for enhancing energy efficiency (Erdoğan and Daşkın, 2023). Figure 1 illustrates a schematic representation of an AHU equipped with a perforated diffuser. According to a market survey among manufacturers of AHUs, there is insufficient information about the flow structure in chambers equipped with perforated diffusers.

Additionally, the perforated diffusers used in AHUs may cause significant noise (Yapanmış, 2016; Erdoğan, 2017). In many instances, this leads to health problems and, as such, is undesirable. Elevated noise levels can also indicate energy inefficiency and vibration problems. The noise generated by perforated diffusers is primarily a result of flow (aeroacoustic) issues. Yapanmış (2016) investigated the pre-emissive properties of perforated diffusers with square truncated pyramid and truncated cone geometries designed for AHUs. The study examined the effects of different geometrical parameters on sound transmission loss. However, it does not cover the aeroacoustic properties of perforated diffusers, focusing instead on their acoustic properties in a flow-free environment. Martinez-Lera et al. (2012) conducted a numerical flow study in an HVAC duct with a flapper inside and subsequently calculated the sound pressure level using the Ffowcs Williams-Hawkings (FW-H) approach in ANSYS-Fluent. Kaltenbacher et al. (2016) presented a novel computational scheme for simulating flow-induced sound in rotating systems. The method, they used, employs scale-resolving simulations with an arbitrary mesh interface, connecting rotating and stationary domains.
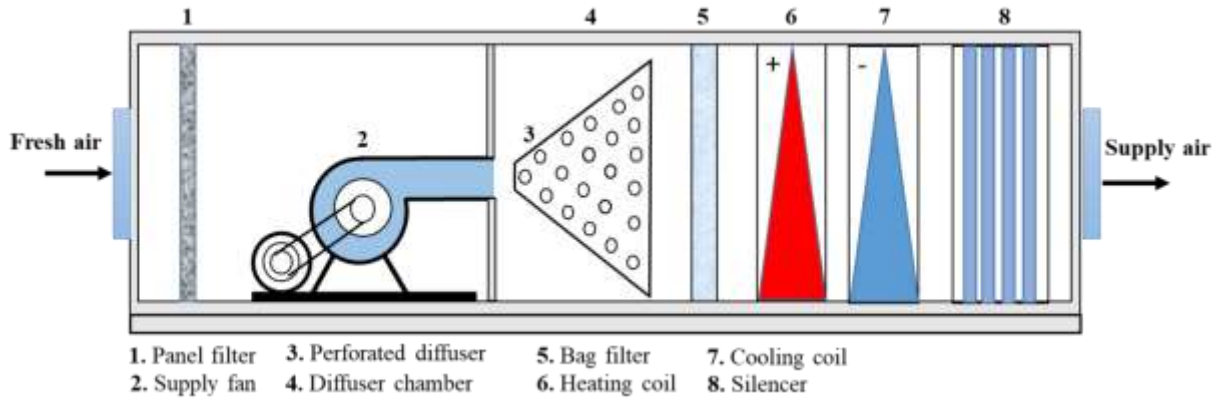
**Figure 1.** Schematic representation of an AHU with perforated diffuser.

The Finite-Element method, along with Nitsche type mortaring, was applied at the interface for solving. They demonstrated in the numerical computation of a side channel blower (Kaltenbacher et al., 2016). Kandekar et al. (2019) investigated flow-induced noise in the 400 Hz to 5000 Hz frequency range and discussed a Computational Aeroacoustics (CAA) approach for simulating. They validated through testing with good correlation between CFD predictions and measurements. Mikedis (2023) performed some numerical simulations on aeroacoustic characteristics in a HVAC duct by employing OpenFOAM CFD toolbox. The Direct Numerical Model (DNS) was used to solve the aeroacoustic simulations and the model was validated with experiments. Bezci numerically investigated the flow structure and aerodynamically induced noise in a centrifugal fan using k-ε and LES (Large Eddy Simulation) turbulence models under five different outlet pressure boundary conditions. Additionally, he determined the noise propagation from the flow in free space using the Ffowcs Williams-Hawkings (FW-H) approach (Bezci, 2009).

Numerous studies in the literature focus on the acoustic performance of silencers equipped with perforated surfaces, employed in diverse industrial applications. Ueda et al. (2002) observed the acoustic field of the resonator through measurements of instantaneous pressure and average velocity. They asserted that the phenomena responsible for sound wave generation and the acoustic resistance of the resonator are closely linked to the phase difference. Furthermore, the efficiency values were found to exhibit a connection at this juncture (Ueda et al., 2002). Emphasizing the significance of designing the grid structure inside the resonator to mitigate pressure fluctuations at the inlet, Zoccola highlighted that an incompatible design with the pressure fluctuation character could result in persistent oscillations. This could even lead to irregular vortex fields instead of periodic ones. Zoccola conducted velocity and sound measurements to establish the relationship between the excitation system, amplitude levels in the resonator, and grid configurations (Zoccola Jr, 2004). Morris et al. concentrated on the pressure

differential, oscillatory excitations, and secondary losses resulting from constrictions and expansions within the resonator flow field. They examined and discussed the interactions between the entire resonator and the expansion and constriction parts separately and in comparison (Morris at al., 2004).

## 2. Materials and Methods

The dimensions of the square truncated pyramid perforated diffuser chamber investigated in this study are shown in Figure 2. All geometric parameters considered in this study are given in Table 1.

**Table 1.** Variable geometric parameters and values

| Parameters | Unit | Value |
|---|---|---|
| $\delta$ | [-] | 0.35, 0.40, 0.45, 0.50, 0.55 |
| $\alpha$ | [°] | 50, 55, 60 |
| $t$ | [mm] | 1, 2, 3 |
| $L_0$ | [mm] | 0, 100, 200 |
| Hole array type | [-] | Staggered, Straight |
| Diffuser surface type | [-] | Flat, convex, concave |
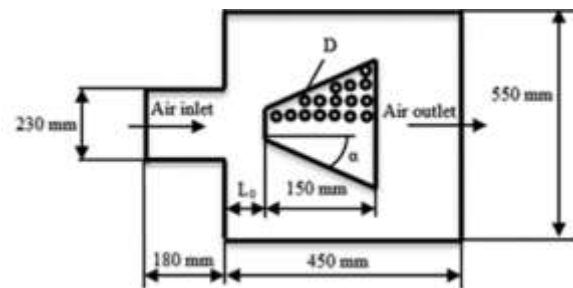


**Figure 2.** The dimensions of the square truncated pyramid perforated diffuser chamber.

In Table 1, '$t$' represents the plate thickness; '$\delta$' indicates the porosity of the perforated diffuser, representing the ratio of the area of apertures to the total surface area of the perforated diffuser; '$\alpha$' and '$L_0$' denote the draft angle of the diffuser and the distance from air inlet to diffuser, respectively. Hole array types are illustrated in Figure 3.
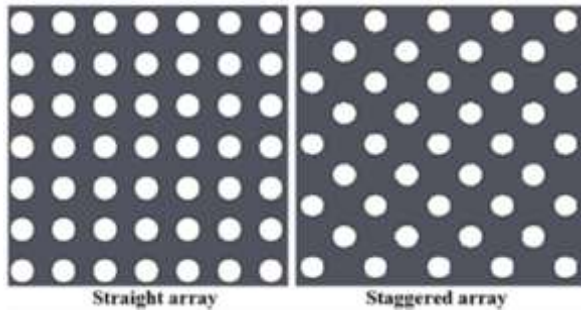
**Figure 3.** Hole array type.

Fluent within the ANSYS software package. Tetrahedral (four-faced) elements, recommended for relatively complex geometries, were employed as the mesh elements (Fluent, 2009). Throughout the surfaces of the perforated diffuser and in the flow domain, the maximum element size was set to 0.01 m, while on the surfaces of the perforated diffuser, it was determined to be 0.005 m. Figure 4 depicts the mesh structure of the CFD models.
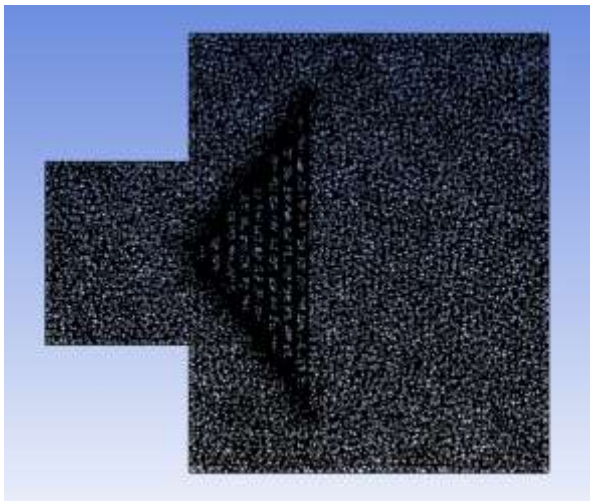


**Figure 4.** Mesh structure of the CFD models.

This study presents the sound pressure levels (SPL) in the chamber with a perforated diffuser in the frequency range of 0-1000 Hz, considering the geometric design parameters of the square truncated pyramid perforated diffuser. The numerical models, developed for aeroacoustic analyses, involved solving Equations 1-5, which represent mass (Equation 1), momentum (Equation 2), and the Standard k-ε turbulence model (Equation 3, 4) in the ANSYS-Fluent software (Fluent, 2009). The simulations were carried out with a time step of 0.0005 s and a total of 1000 time steps. The boundary conditions include a "velocity inlet" defined for the 230 mm x 230 mm air inlet section, and a "pressure outlet" defined for the 550 mm x 730 mm air outlet section. The air inlet velocity is assumed to be 16.2 m/s, while the average static pressure at the outlet section is assumed to be 100 Pa. Subsequently, employing the Fowcs Williams-Hawkings (FW-H) approach within the Ansys-Fluent program, based on the Lighthill acoustic analogy,

time-dependent acoustic signals were acquired from three microphones strategically placed within the chamber. The SPL values were then determined across frequencies using the Fast Fourier Transform (FFT) module in the CFD-Post section. The microphone positions placed inside the square truncated pyramid hole diffuser chamber, here presented as microphone 1-M1, microphone 2-M2, and microphone 3-M3, are shown in Figure 5.

$$\frac{\partial u_i}{\partial x_i} = 0 \tag{1}$$

$$\frac{\partial\, u_i u_j}{\partial x_j} = -\frac{\partial p}{\partial x_i} + \frac{\partial}{\partial x_j}\left[\mu\left(\frac{\partial u_i}{\partial x_j} + \frac{\partial u_j}{\partial x_i}\right)\right] - \frac{\partial}{\partial x_j}(\rho\, \overline{u_i' u_j'}) \tag{2}$$

where $u$ and $p$ are the velocity and pressure, respectively. $\overline{u_i' u_j'}$ states Reynolds stress.

$$\frac{\partial(\rho k)}{\partial t} + \frac{\partial(\rho k u_i)}{\partial x_i} = \frac{\partial}{\partial x_j}\left[\left(\mu + \frac{\mu_t}{\sigma_k}\right)\frac{\partial k}{\partial x_j}\right] + G_k - \rho\varepsilon \tag{3}$$

$$\frac{\partial(\rho\varepsilon)}{\partial t} + \frac{\partial(\rho\varepsilon u_i)}{\partial x_i} = \frac{\partial}{\partial x_j}\left[\left(\mu + \frac{\mu_t}{\sigma_\varepsilon}\right)\frac{\partial\varepsilon}{\partial x_j}\right] + C_{1\varepsilon}\frac{\varepsilon}{k}G_K - C_{2\varepsilon}\rho\frac{\varepsilon^2}{k} \tag{4}$$

In equation 3 and equation 4, the symbols $k$ and $\varepsilon$ represent turbulence kinetic energy and turbulence dissipation rate, respectively. The turbulent viscosity, denoted as $\mu_t$, is expressed through the calculated Equation 5 presented below.

$$\mu_t = \rho C_\mu \frac{k^2}{\varepsilon} \tag{5}$$

The constants in these equations are assigned the following values, respectively: $\sigma_k$=1, $\sigma_\varepsilon$=1.3, $C_{1\varepsilon}$=1.44, $C_{2\varepsilon}$=1.92, and $C_\mu$=0.09 (Fluent, 2009).
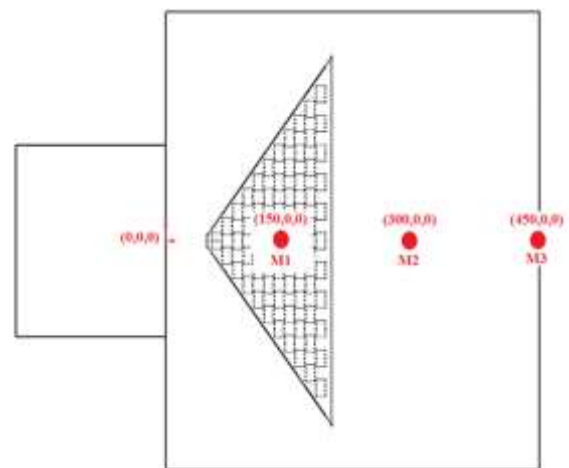


**Figure 5.** Microphone positions in chamber with perforated diffuser.

## 3. Results and Discussion

The CFD analyses conducted to investigate the impact of the geometrical design parameters of the square

truncated pyramid perforated diffuser on the SPL generated by the airflow within the chamber involved collecting data from microphones at three distinct locations across the frequency range of 0-1000 Hz. Figure 6 shows the porosity effect on the SPL. Upon analyzing Figure 5, it is noted that the variation in SPL with different porosity values differs depending on the position of the receiving microphone. Generally, however, the SPL within the chamber equipped with a perforated diffuser increases as the porosity value rises. Reducing the porosity value from 0.55 to 0.35 can result in a significant noise reduction in SPL, amounting to approximately 30-40 dB across nearly all frequency values. In the context of this flow model, it can be inferred that higher porosity values lead to increased SPL values due to the formation of more vortices in the flow domain. Figure 7 illustrates the impact of the diffuser draft angle on the SPL. According to Figure 7, a decrease

in SPL near the diffuser is observed as the draft angle increases. Specifically, signals from M1, positioned closest to the diffuser, consistently exhibit lower SPL values, except for certain frequency values observed in signals from M3, located farthest from the diffuser, for $\alpha$=55°. Additionally, an increase in the draft angle induces greater fluctuations in SPL across various frequencies. The impact of the specified diffuser wall thickness values on the SPL is depicted in Figure 8. Upon analysis, it is noted that there is a decline in the SPL with an increase in the wall thickness parameter from 1 mm to 2 mm for signals received from M1, the microphone closest to the diffuser. However, in the case of signals received from microphones M2 and M3, it is observed that the SPL is higher at the intermediate value of 2 mm wall thickness compared to the values of 1 mm and 3 mm.
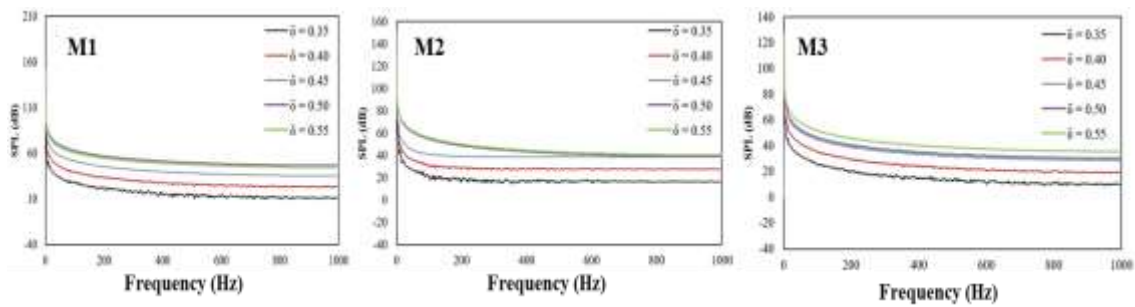


**Figure 6.** Porosity effect on SPL.
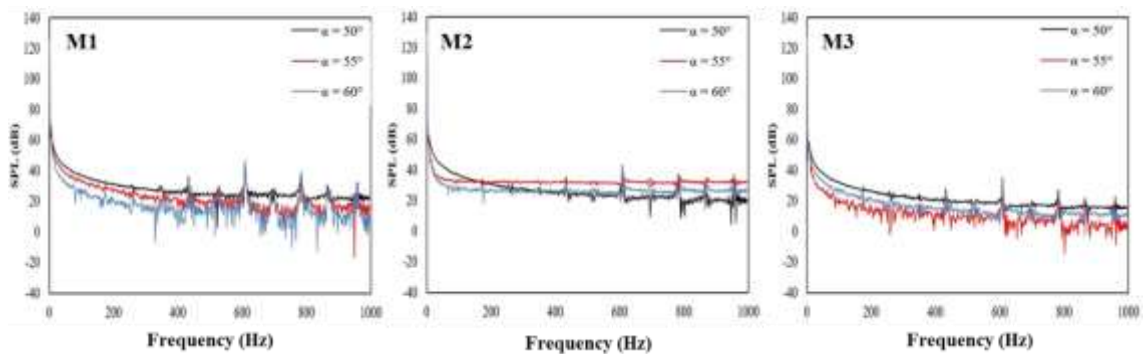


**Figure 7.** Draft angle effect on SPL.
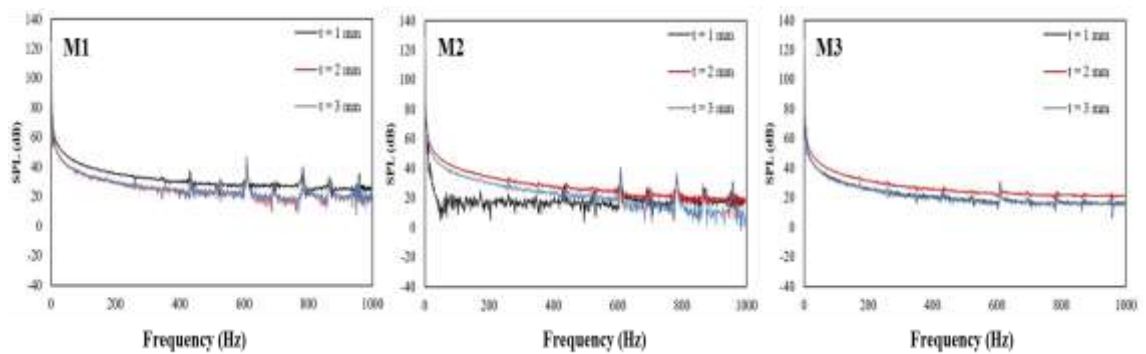


**Figure 8.** Diffuser thickness effect on SPL.

Figure 9 illustrates a graph depicting the variation in SPL with the position of the square truncated pyramid

perforated diffuser ($L_0$) within the chamber. Examination of this graph reveals a substantial correlation between

the diffuser position and the microphone position in the obtained signal values. Specifically, it is observed that the SPL is higher at $L_0$=100 mm in the signals received from the M1 receiver. This is attributed to the fact that the M1 microphone position is 50 mm inside the peak of the perforated diffuser, where the noise caused by the time-dependent vortical flow structure is more pronounced. Figure 10 gives the SPL values acquired for various hole array types and three different microphone positions. With the exception of some signal values obtained from

the M2 receiver at low frequencies, it is evident that the staggered array results in higher SPL than the straight placement type for all three microphone positions. Figure 11 presents the SPL values recorded from three distinct microphone positions when the surface type of the perforated diffuser is flat, convex, and concave. Based on the signals obtained from the microphone in all three positions, it can be concluded that the concave geometry induces more fluctuations in the SPL across different frequencies and results in a lower overall SPL.
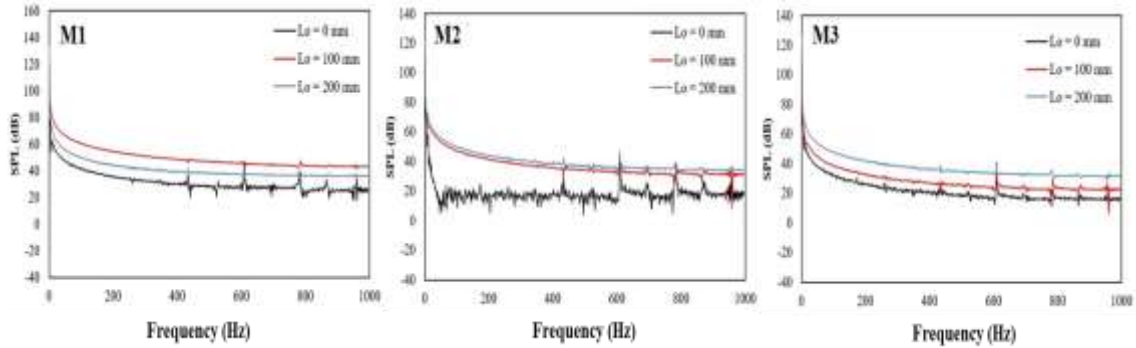


**Figure 9.** Diffuser locations effect on SPL.
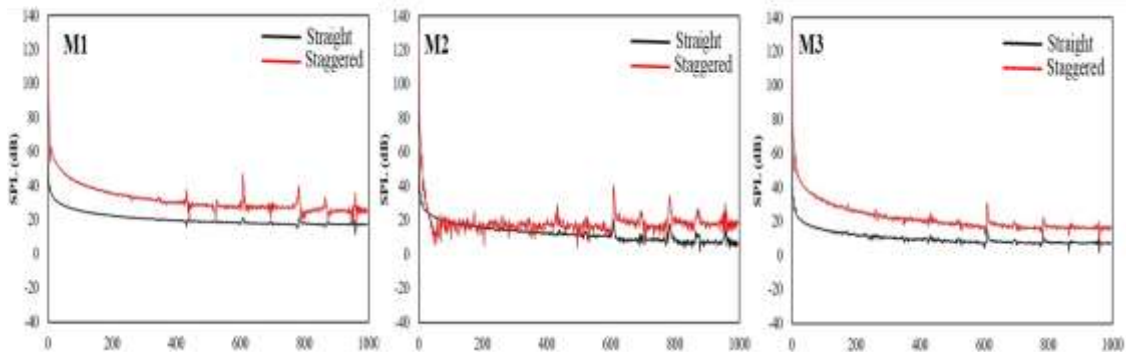


**Figure 10.** Hole array type effect on SPL.
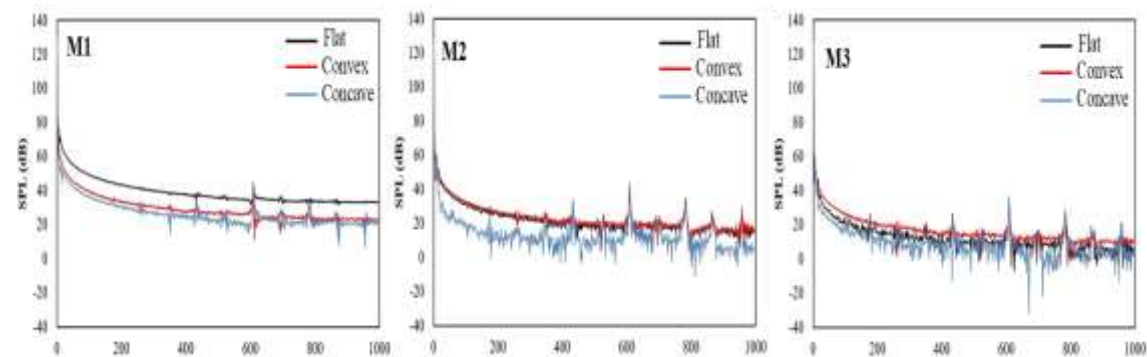


**Figure 11.** Diffuser surface type effect on SPL.

## 4. Conclusion

This study offers insights into how the geometric parameters of square truncated pyramid perforated diffusers, utilized in AHU, influence the SPL. Following CFD-based aeroacoustic analyses, SPL values were acquired within the frequency range of 0-1000 Hz for each geometric parameter value employed in the diffuser configuration.

- Low porosity value provides lower SPL values. A reduction in porosity from 0.55 to 0.35 can drastically reduce SPL by approximately 30-40 dB across almost all frequency ranges.
- While the SPL decreases with a reduction in the draft angle for the M2, a draft angle of 55° results in less noise, approximately 20 dB lower, compared to values obtained from microphones positioned (M3)

farther from the diffuser.

- Analyzing signals from the microphone in the downstream region of the diffuser revealed that the impact of wall thickness variation on SPL fluctuated at each frequency value, typically within a range of 5-10 dB.
- The placement of the diffuser within the chamber (L0) can influence the SPL by approximately 20 dB, regardless of the microphone's position. When the diffuser is positioned near the air inlet surface (L0=0), the lowest SPL is achieved downstream of the diffuser.
- The straight array results in a reduction in SPL of approximately 20 dB at all microphone positions compared to the staggered array.
- Analyzing signals from the microphone located downstream of the diffuser, it is observed that when the diffuser surface is flat, concave, or convex, there is a maximum difference of 5 dB in SPL across different frequencies.

As a future study, the fluid domain in these CFD models will be expanded to include the HVAC duct component. Consequently, the microphone positions will be relocated to align with the new model. Additionally, other AHU components, such as the heating/cooling coil, humidifier, and filter, will be integrated into the models. This expansion aims to yield more comprehensive results.

## Author Contributions

The percentage of the author(s) contributions is presented below. All authors reviewed and approved the final version of the manuscript.

|     | A.E. | İ.G.A. | S.C. |
|-----|------|--------|------|
| C   | 40   | 30     | 30   |
| D   | 60   | 20     | 20   |
| S   | 60   | 20     | 20   |
| DCP | 80   | 10     | 10   |
| DAI | 60   | 20     | 20   |
| L   | 50   | 25     | 25   |
| W   | 50   | 25     | 25   |
| CR  | 40   | 30     | 30   |
| SR  | 80   | 10     | 10   |
| PM  | 30   | 35     | 35   |
| FA  | 20   | 40     | 40   |

C=Concept, D= design, S= supervision, DCP= data collection and/or processing, DAI= data analysis and/or interpretation, L= literature search, W= writing, CR= critical review, SR= submission and revision, PM= project management, FA= funding acquisition.

## Conflict of Interest

The authors declared that there is no conflict of interest.

## Ethical Consideration

Ethics committee approval was not required for this study because of there was no study on animals or humans.

## References

Bezci H. 2009. Aeroacoustic properties of a radial fan. PhD Thesis, İstanbul Technical University, Institute of Science and Technology, İstanbul, Türkiye, pp: 85.

Bulut S, Unveren M, Arisoy, A, Boke, Y. 2011. Reducing internal losses in air handling units with CFD analysis method. TMMOB X. National Plumbing Engineering Congress and Exhibition, April 11-13, İzmir, Türkiye, pp: 291-326.

Erdoğan A, Daşkın M. 2023. Comparing of CFD contours using image analysing method: A study on velocity distributions. BSJ Eng Sci, 6(4): 633-638.

Erdoğan A. 2017. Investigation of airflow in empty chambers with perforated diffuser designed for air handling units in terms of flow and acoustic. PhD Thesis, İnönü University, Institute of Science, Malatya, Türkiye, pp: 115.

Fluent A. 2009. 12.0 User's guide. Ansys Inc, 6: 552.

Kaltenbacher M, Hüppe A, Reppenhagen A, Tautz M, Becker S, Kuehnel V. 2016. Computational aeroacoustics for HVAC systems utilizing a hybrid approach. SAE Int J Passeng Cars Mech, 9(3): 1047-1052.

Kamer MS, Erdoğan A, Taçgün E, Sonmez K, Kaya A, Aksoy IG, Canbazoglu S. 2018. A performance analysis on pressure loss and airflow diffusion in a chamber with perforated V-profile diffuser designed for air handling units (AHUs). J Appl Fluid Mech, 11: 1089-1100.

Kandekar A, Nagarhalli P, Dol Y, Thakur S, Gupta B, Jadhav T. 2019. HVAC system noise prediction through CFD simulation. SAE Tech Pap, 26: 210.

Martinez-Lera P, Hallez R, Bériot H, Schram, C. 2012. Computation of sound in a simplified HVAC duct based on aerodynamic pressure. 18th AIAA/CEAS Aeroacoustic Conference (33rd AIAA Aeroacoustic Conference), June 4-6, Colorado, US, pp: 1-10.

Mikedis K. 2023. Prediction of aerodynamically induced noise in automotive HVAC systems. Diploma Thesis, National Technical University, Athens School of Mechanical Engineering, Athens, Greece, pp: 93.

Morris PJ, Boluriaan S, Shieh CM. 2004. Numerical simulation of minor losses due to a sudden contraction and expansion in high amplitude acoustic resonators. Acta Acust United Acust, 90: 393-409.

Ueda Y, Biwa T, Mizutani U, Yazaki T. 2002. Acoustic field in a thermoacoustic Stirling engine having a looped tube and resonator. Appl Phys Lett, 81: 5252-5254.

Yapanmış BE. 2016. Design of perforated diffuser as a pre-silencer. PhD Thesis, Mersin University, Institute of Science, Mersin, Türkiye, pp: 95.

Yu Y, Woradechjumroen D, Yu, D. 2014. A review of fault detection and diagnosis methodologies on air-handling units. Energy Build, 82: 550-562.

Zoccola Jr JP. 2004. Effect of opening obstructions on the flow-excited response of a Helmholtz resonator. J Fluids Struc, 19: 1005-1025.